*Desalination and Water Treatment*
www.deswater.com

doi: 10.5004/dwt.2021.26581

210 (2021) 22–30
January

# Photodegradation of mefenamic acid from wastewater in a continuous flow solar falling film reactor

Zainab Yousif Shnain[a], Mohammad Fadhil Abid[b,*], Khalid A. Sukkar[a]

[a]*Department of Chemical Engineering, University of Technology, Baghdad, Iraq, email: 80062@uotechnology.edu.iq (Z.Y. Shnain), khalid.a.sukkar@uotechnology.edu.iq (K.A. Sukkar)*

[b]*Department of Medical Instrumentation Engineering, Al-Hikma University College, Baghdad, Iraq, email: mohammad.abid@hiuc.edu.iq*

Received 4 April 2020; Accepted 15 September 2020

**ABSTRACT**

The degradation of mefenamic acid (MFA) in synthetic wastewater was studied utilizing homemade Cu-doped $TiO_2$ nanoparticles in a solar-irradiated falling film reactor. Energy-dispersive X-ray spectroscopy and scanning electron microscopy analyses were applied to identify the homemade Cu-doped $TiO_2$ nanocatalyst. Adsorption experiments revealed that the Langmuir isotherm model well-described the experimental data. Various operating parameters, such as loadings of MFA (10–75 mg $L^{-1}$), doped catalyst (300–800 mg $L^{-1}$), $H_2O_2$ (300–800 mg $L^{-1}$), synthetic wastewater flow rate (1–3 L $min^{-1}$), and wastewater pH (3–10), have been investigated for their effects on MFA degradation. A degradation of MFA of 97.5% was achieved within 90 min of the operation period by operating at pH = 10, $C_{CU-TiO_2}$ = 400 mg $L^{-1}$, $C_{H_2O_2}$ = 400 mg $L^{-1}$, and $Q_{sw}$ = 1.0 L $min^{-1}$. The experimental results revealed that an enhancement of 50.09% for degradation of MFA was attained by the 2wt.% Cu-doped $TiO_2$ higher than pure $TiO_2$.

*Keywords:* Solar irradiation; Falling film reactor; Pharmaceuticals; Photocatalysis; Wastewater

## 1. Introduction

Mefenamic acid (MFA) is a nonsteroidal anti-inflammatory medicine. It is prescribed medication for menstrual pain [1]. It is charged orally. Fig. 1 depicts the chemical structure.

Wastewater effluent from some Iraqi hospitals contains unacceptable ingredients of pharmaceuticals which threaten the aquatic environment if they are not being removed [2]. Published data have monitored analgesics in wastewater effluent. Research on toxicity reported that exposure to MFA can highly motivate untoward influences on aqueous living creatures like luminescence suppression, change of swim performance, and doom [3–5]. The basics of heterogeneous photocatalysis encompass the utilizing of a rigid semiconductor, like ZnO, and $TiO_2$ so as to shape a constant suspension at the effect of irradiation to promote a reaction at the interface of the two phases in the operating system. Recently, $TiO_2$ is considered the best semiconductor in the heterogeneous photoinduced treating. Degradation of organic pollutants by heterogeneous photoinduced reaction (HPR) is the most workable implementations of the advanced oxidation processes as proposed by a vast variety of literature concerning the removal of toxic organics in water [6]. As seen in Fig. 2, upon UV-solar incident irradiation, $e^-$–$h^+$ pairs are generated on $TiO_2$ surface. These pairs are when combining with $H_2O$ molecules in the presence of dissolved oxygen, the following radicles and ions are formed, hydroxyl radical ($^{\bullet}OH$) and superoxide radical ($O_2^{-\bullet}$). These radicals destroy many toxins bonds that existed in the solution [7].

The undoped $TiO_2$ that utilizes UV spectrum to motivate the photoinduced process has a bandgap near 3.2 eV. To beat an obstacle of bandgap (~3.2 eV) for pure $TiO_2$ that utilizes the UV spectrum to motivate the photocatalytic

* Corresponding author.

This article was originally published with an error in the names of the first and third authors. This version has been corrected.
Please see Corrigendum in vol. 214 (2021) 453 [doi: 10.5004/dwt.2021.27167] and in vol. 218 (2021) 455 [doi: 10.5004/dwt.2021.27277]

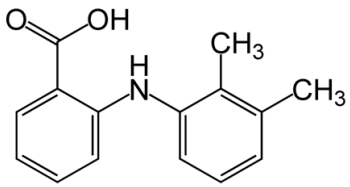


Fig. 1. Chemical structure of MFA.

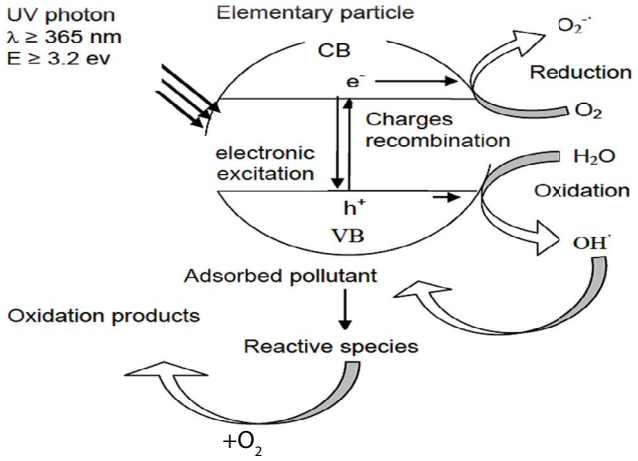


Fig. 2. Mechanism of photocatalytic degradation in presence of UV radiation.

degradation, many endeavors were achieved to transfer the excitation of $TiO_2$ nanoparticles into the visible zone by reducing the bandgap, thus allowing the utilization of solar light for photodegradation [8]. Copper oxides display narrow bandgap (1.4–2.3 eV) substance which has higher absorptivity. However, it undergoes from photo corrosion. It was reported that copper oxides combined with $TiO_2$ offered more stability with higher photocatalytic effectiveness. Many researchers [9–15] studied the degradation of toxic materials generated from different activities (e.g., xylene, pharmaceuticals, phenol, and pesticides) using the homogeneous or the coupled homogenous–heterogeneous photocatalytic process under a stable UV or time-dependent solar irradiated reactor at different operating variables like pH of the solution, loading of a heterogeneous catalyst, loading of a homogeneous catalyst, $H_2O_2$ loading, and liquid flow rate. Gimeno et al. [16] investigated the removal of MFA by photolysis, ozonation, adsorption onto activated carbon (AC) by the systems ($O_3$+AC and $O_3$+UV). They reported that MFA has not been found photo-sensitive. Sankoda et al. [17] studied experimentally the photochemical decomposition of MFA and triclosan in synthetic wastewater. The authors revealed that MFA was subjected to indirect photolysis by reactive by-products that formed in wastewater. The authors proposed that generated (•OH) and stimulated dissolved organic compound boost the decay of MFA. Dolatabadi et al. [18] studied the degradation of MFA being discharged from clinical centers utilizing the electro-Fenton (E-Fenton) technique in a Pyrex reactor. The authors reported that the removal efficiency of 95.3% was attained at the optimum operating variables. The current research aimed to study using a solar-irradiated falling film catalytic reactor to degrade MFA in synthetic wastewater under the effect of different operating parameters such as mode of flow, solar irradiation intensity, the acidity of the solution, $H_2O_2$ loading, and concentration of a homemade 1 wt.% Cu-doped $TiO_2$ photocatalyst in solution.

## 2. Materials and methods

### 2.1. Materials

Titanium isopropoxide [Ti-(OCH(CH3)2)4] (purity 99.99%) was supplied from ChemPure (India). $CuSO_4{\cdot}5H_2O$ (98% min) was obtained from Alfa Aesar (Indonesia). Analytical grade MFA was suppled from Sigma-Aldrich (Merck Serono Iraq). Hydrogen peroxide (30%) was obtained from Arkema (Turkey). HCl (36%), NaOH (flakes, 99 wt.%), NaCl (powder, 99 wt.%), and RO water were supplied from the local market. The chemical properties of the RO water are (pH = 6.8, TDS = 20 mg $L^{-1}$, total hardness = 60 mg $L^{-1}$, and conductivity = 21 μS $m^{-1}$).

### 2.2. Methods

#### 2.2.1. Catalyst preparation

To synthesize 0.5 and 2 wt.% Cu-doped $TiO_2$, $CuSO_4{\cdot}5H_2O$ of different weights were dissolved in liquid ammonium hydroxide (25 wt.%) to form 0.25 and 1 M of CuSO4 solutions respectively. One millimeter of titanium isopropoxide was mixed with the prepared $CuSO_4$ solution and the mixture was subjected to ultrasonic waves induced by an ultrasonic generator (Model VCX-750, Vibra-cell, Sonics) for 30 min with a break of 3 min between each 5 min of ultrasonication period. The precipitate formed is washed 3–4 times with ethanol and acetone mixture to remove organic components. The precipitate was kept for drying for 1 h at 100°C. Finally, as-prepared Cu-doped $TiO_2$ materials annealed for 60 min. at ~500°C. In addition, pure $TiO_2$ was synthesized using the same synthesis steps.

#### 2.2.2. Catalyst characterization

The surface characteristics were performed by utilizing a Tescan VEGA 3SB scanning electron microscopy (SEM) with a voltage of 200 V–30 kV and an enlargement capacity from 4X to $10^5$X. Chemical ingredients of the homemade semiconductor were elucidated by utilizing the energy-dispersive X-ray spectroscopy (EDS) model; inspect S50/FEI Company, Netherland. The pH of the slurry was measured by pH meter (pH 500 from FALC Instrument, Italy) with a calibrated glass-Ag/AgCl electrode.

#### 2.2.3. Experimental rig and procedure

Figs. 3a and b show a scheme and a photo image of the rig. The setup includes a solar reactor (No. 6), a 5 L-PVC feed tank (No. 1), a pump (No. 3), type: KSB (Model Calio S, Head = 6 m, flow rate up to 3.5 $m^3$ $h^{-1}$). The solar reactor was installed on a podium inclined with 37° and guided south–east. The reactor consisted of transparent flat glass of dimensions 1,100 mm × 800 mm × 4 mm. It was mounted

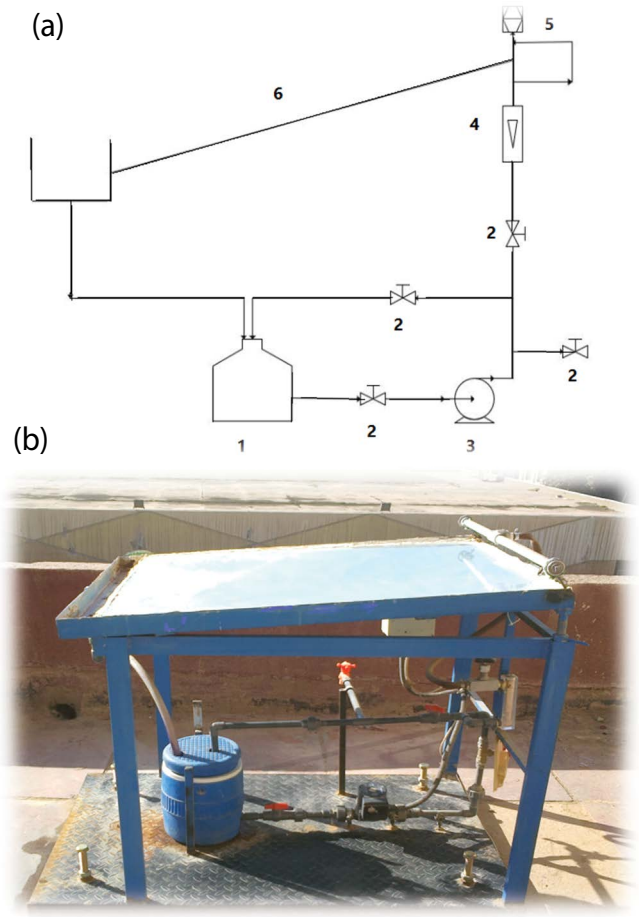


Fig. 3. Experimental setup (a) scheme and (b) photographic image. (1) Waste water vessel, (2) regulating valve, (3) pump, (4) flow meter, (5) liquid distributor, and (6) glass flat plate.

on a chrome-coated steel plate. This arrangement makes the light entering the liquid film reflecting by the chrome-coated sheet can also be utilized for the photolysis reaction taking place in the liquid film. The pump was utilized to charge the reactor with synthetic wastewater, synthesized from MFA and RO water, from the tank through a calibrated liquid stream meter (No. 4). The solution trickled down from a tube (No. 5), which has several holes, mounted on the frame of the tilted transparent glass. The mixture temperature was monitored using a thermocouple type (pt-100). In addition, to enhance the solubility of gaseous oxygen in the synthetic wastewater an electric-driven mixer was utilized which help also for homogenizing the wastewater in the tank. Samples were taken at the reactor outlet then analyzed for MFA by the UV-vis 1601 Shimadzu spectrophotometer. The tests were performed according to the UV absorbance maxima at 288 nm wavelength of MFA with RO water utilized as a solvent. Due to the constraints in the spectrophotometer, all the samples were diluted in the ratio 1:10. To form a graphical relation between MFA concentration in wastewater and its correspondent light absorbency, various samples containing MFA loading of 5, 10, 30, 80, 100, and 200 mg $L^{-1}$ were prepared. Fig. 4 illustrates the calibration curve.

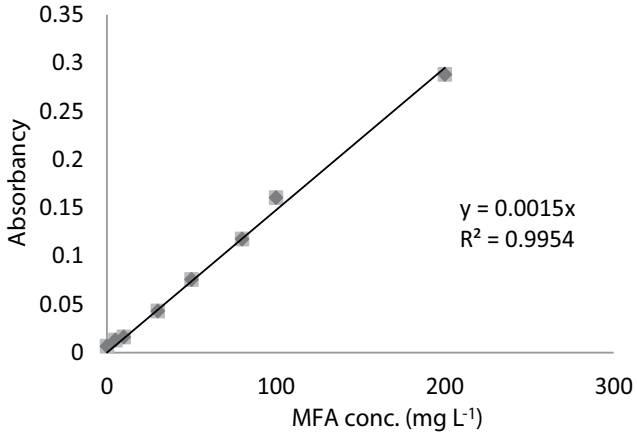


Fig. 4. Calibration curve of MFA.

#### 2.2.4. Experimental design

Planning of experimental runs was arranged utilizing the factorial method in the current study, because of its reliability [19]. Table 1 lists the actual operating parameters ($F$) with their levels ($L$).

## 3. Results and discussion

### 3.1. Light absorbency measurement

Cu-doped $TiO_2$ nanoparticles with different wt.% of Cu (0%, 0.5%, and 2%) were synthesized and UV-VIS absorbance of doped and undoped $TiO_2$ was measured using UV-vis 1601 Shimadzu spectrophotometer. The bandgap energy of the nano photocatalyst is calculated according to the formula $E = hc/\lambda$ [20] where $h$, $c$, and $\lambda$ are Blank constant (= $4.1357 \times 10^{-15}$ eV s), light velocity (= $2.99705 \times 10^{8}$ m $s^{-1}$), and wavelength (nm) respectively. Absorbance data for the samples are listed in Table 2. It shows a shift in wavelength from UV to the visible region. The absorbance values start increasing as the Cu loading is increased.

### 3.2. Surface morphology and structure of Cu-doped $TiO_2$ catalyst

#### 3.2.1. EDS analysis

The compositions of $TiO_2$ and the impurities on the surface of the synthesized catalyst have been identified with the EDS techniques shown in Fig. 5. The $x$-axis of the EDS image signalizes the ionization energy and the $y$-axis signalizes the counts. The more the altitude of counts of a specific element, the more is existence of that element at that zone of consideration. The comparability of pure $TiO_2$ (Fig. 5a) with 2 wt.% Cu-doped $TiO_2$ (Fig. 5b), depicts the peaks shown in the image of 2 wt.% Cu-doped $TiO_2$ confirm the existence of Cu metal with reasonable content of $TiO_2$ atoms. This distinctly exhibits the Cu-doping inside the $TiO_2$ lattice.

#### 3.2.2. SEM analysis

The actual size of the particle can be straightway detected by SEM monitoring. SEM images of 2 wt.%

Table 1
Chosen factors and their levels

| *F* / *L* | Real variables | | | | |
|---|---|---|---|---|---|
| | MFA concentration (mg $L^{-1}$) | Liquid flow rate (L $min^{-1}$) | pH (–) | $H_2O_2$ loading (mg $L^{-1}$) | $TiO_2$ loading (mg $L^{-1}$) |
| 1 | 10 | 0.5 | 5 | 200 | 200 |
| 2 | 30 | 1.0 | 7 | 300 | 400 |
| 3 | 45 | 2.0 | 9 | 400 | 600 |
| 4 | 75 | 3.0 | | 500 | 800 |

Table 2
Effect of Cu doping on the bandgap energy of the photocatalyst

| Item | wt.% Cu-doping | Wavelength (nm) | Energy bandgap (eV) |
|---|---|---|---|
| 1 | 0.0 | 387 | 3.20 |
| 2 | 0.5 | 410 | 3.04 |
| 3 | 2.0 | 563 | 2.20 |

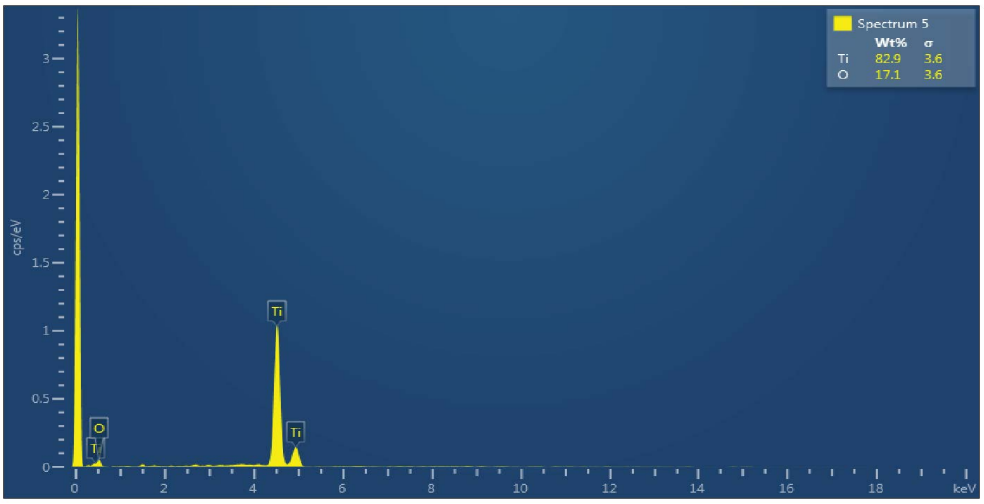


**(a)**

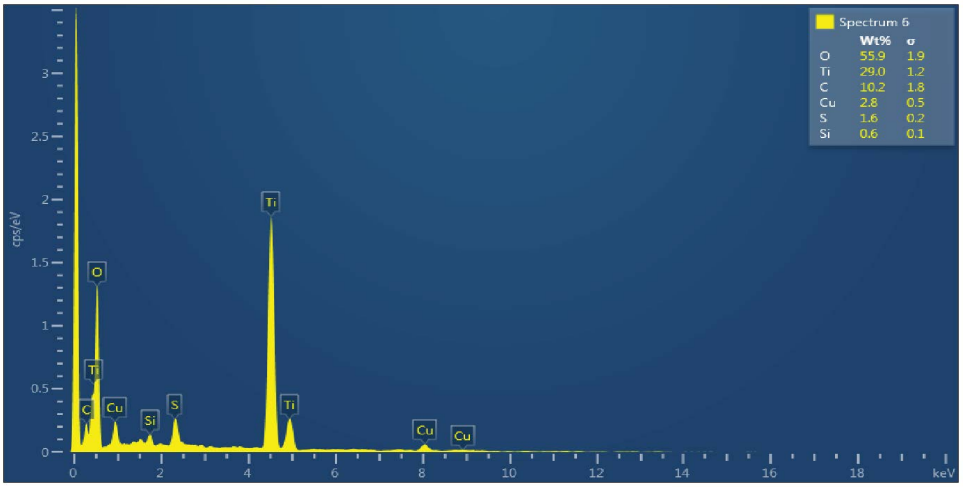


**(b)**

Fig. 5. EDS snapshots of (a) pure $TiO_2$ and (b) 2 wt.% Cu-doped $TiO_2$.

Cu-doped $TiO_2$ are seen in Fig. 6a (SEM Mag.: 1.00 kx) and Fig. 6b (SEM Mag.: 2.00 kx). The images depict a number of aggregated nanocrystallites jointly with the size of nano $TiO_2$ as 57.84 nm. As observed in Fig. 6, Cu powder was nearly distributed equally on the $TiO_2$ surface.

### 3.3. Measurement of point of zero charge

Determination of the PZC of metal oxides is of importance to predict their behaviors in an alkaline or acidic solution for mass transport or kinetic mechanisms [21]. In the present study, the PZC of synthesized Cu-doped $TiO_2$ was measured using the electrolyte titration method published by [22]. Initial $TiO_2$ slurry was prepared by adding an amount of 100 g to an aqueous HCl solution of the amount of $3.65 \times 10^{-2}$ g HCl $L^{-1}$ of RO water. NaCl powder was added gradually to the slurry so that ionic strength has been raised from $10^{-4}$ to 1.0 mol $L^{-1}$. The pH of the slurry was monitored after each addition of NaCl and after (5 min under ultrasound and 10 min of stirring). At relatively high ionic strengths of $10^{-3}$ and 1.0 mol $L^{-1}$, the $pH_{pzc}$ = 6.2. While at a low ionic strength of $10^{-4}$ mol $L^{-1}$, has a $pH_{pzc}$ of 5.9. An average $pH_{pzc}$ = 6.1 was considered in our work with a percentage relative error of 1.5%.

### 3.4. Adsorption experiments

The ultimate uptake ability of 2 wt.% doped-$TiO_2$ was evaluated by performing adsorption runs at different pH (5, 7, and 9). Different concentrations (5, 10, 20, 30, 40, and 50 ppm) of an aqueous solution of MFA in RO water were synthesized. Then 100 mL of each concentration is put in a 250 mL beaker separately with 1 g of doped-$TiO_2$. The amount of MFA adsorbed at equilibrium, (mg $g^{-1}$) was evaluated utilizing Eq. (1) [23].

$$q_e = \frac{\left(C_0 - C_e\right)V}{W} \tag{1}$$

where $C_0$ and $C_e$ are the concentrations of MFA at initial and at equilibrium (mg $L^{-1}$), respectively, $V$ is the volume of solution, and $W$ is the mass of doped-$TiO_2$ used (g). The Langmuir model is vastly used for isotherms, the correlation of Langmuir isotherm [24] is expressed by Eq. (2):

$$q_e = \frac{q_m \cdot K_L \cdot C_e}{\left(1 + K_L \cdot C_e\right)} \tag{2}$$

where $q_m$ is the maxima quantity of metal V adsorbed per unit mass of zeolite (mg $gm^{-1}$), $q_e$ is the concentricity of MFA at equilibrium (mg $L^{-1}$). $K_L$ is the Langmuir constant (L $mg^{-1}$). Fig. 7 plots the experimental results of MFA adsorption at equilibrium onto 2 wt.% Cu-doped-$TiO_2$ at different pH after 2 h.

Eq. (3) represents the linearized form for Eq. (2):

$$\frac{1}{q_e} = \frac{1}{q_m} + \frac{1}{K_L q_m C_e} \tag{3}$$

Fig. 8 shows a plot of $\frac{1}{q_e}$ vs. $\frac{1}{C_e}$ with a correlation coefficient ($R^2$) = 0.9943 by Eq. (4) representing a best-fit line:

$$y = 0.0217x + 0.0123 \tag{4}$$

From Eq. (7), $q_m$ = 81.3 mg $g^{-1}$ and $K_L$ = 1.0106 L $mg^{-1}$.

These results assure the viability of Langmuir isotherm in our study. This outcome depicts that the maximum uptake of MFA was = 3 9.35 mg $g^{-1}$ at pH = 9, this may be attributed to the capability of the usable doped-$TiO_2$ structural frame with a high percentage of the pore volume.

### 3.5. Effect of operating parameters on degradation of MFA

All figures (except Fig. 13) in section 3.5.4 were plotted for MFA decomposition as a function of incident solar energy. The accumulate energy per unit volume of synthetic

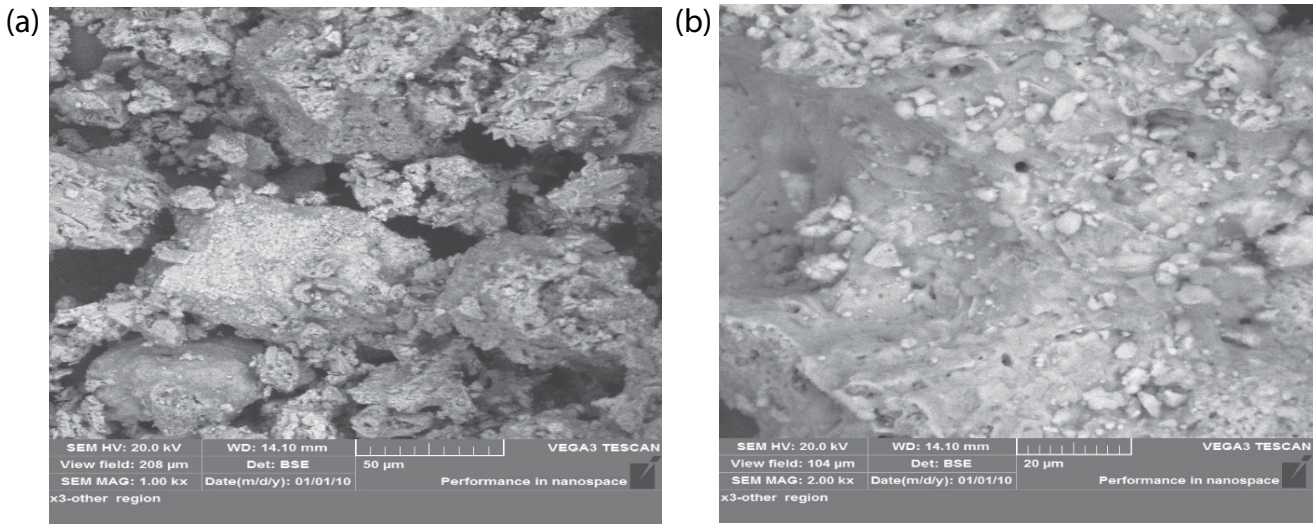


Fig. 6. (a and b) SEM images of 2 wt.% Cu-doped $TiO_2$.

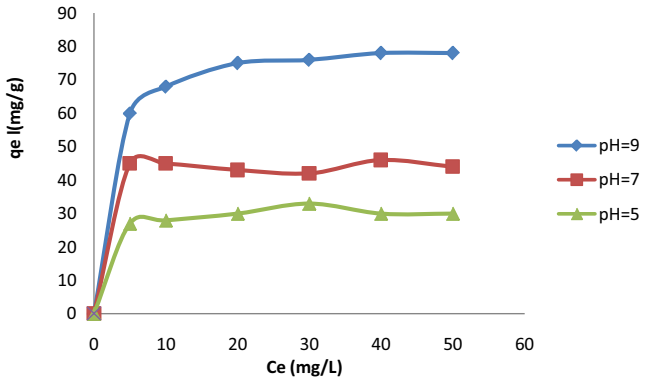


Fig. 7. Adsorption data of MFA onto 2 wt.% Cu-doped-$TiO_2$ at different pH after 2 h.

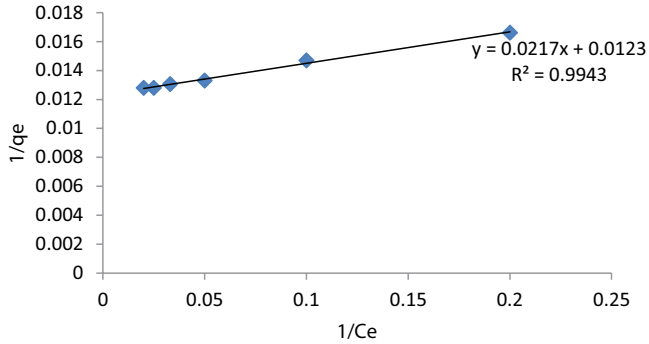


Fig. 8. Linearization plot of the Langmuir model for equilibrium adsorption of MFA on doped $TiO_2$ at pH = 9.

wastewater flow ($Q_{UV,n}$) across the solar reactor at the $n$th sample was estimated using Eq. (5) [11]:

$$Q_{UV,n} = Q_{UV,n-1} + \Delta t_n \times UV_{GN} \times \frac{A}{V} \quad (5)$$

where $\Delta t$ is the time interval between each sample (15 min), $A$ is the irradiated area of the reactor (800 × 110) $cm^2$, $V$ is the volume of synthetic wastewater in the system = 5 L, $n$ is the number of samples, and $UV_{GN}$ is the average local-global UV irradiation = 33.7 W $m^{-2}$.

### 3.5.1. Influence of pH

Fig. 9 clarifies the change of %$R$ with cumulative ultraviolet energy per liter of solution ($Q_{UVS}$) in the reactor outlet at different pH after 90 min. The initial pH of synthetic wastewater was varied from 3 to 10 with all other operating variables were kept constant at ($C_{MFA}$ = 10 mg $L^{-1}$, $C_{H_2O_2}$ = $C_{Cu-TiO_2}$ = 400 mg $L^{-1}$, $Q_{sw}$ = 1.0 L $min^{-1}$). In Fig. 9, it is observed that after 90 min of solar illumination, the values of %$R$ attained 49.5, 58. 8, 72.2, 88, and 97.5 as the incipient pH of the solution was 3, 5, 7, 8, and 10, respectively. This behavior may be attributed to the surface charge of $TiO_2$. According to Eq. (6), the pKa (the negative log of the MFA dissociation constant) = 4.2 [25].

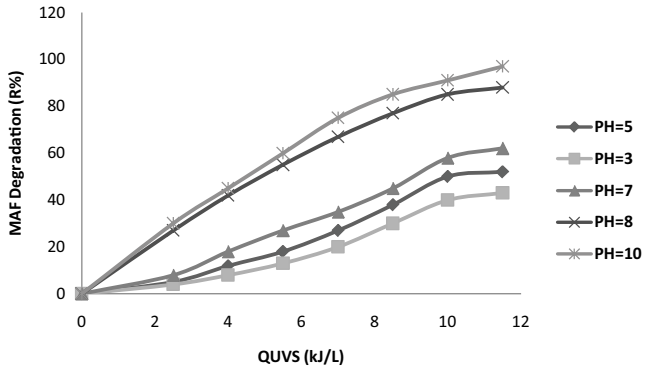


Fig. 9. Variation of %$R$ against $Q_{UVS}$ (kJ $L^{-1}$) in reactor effluent at different pH after 90 min.

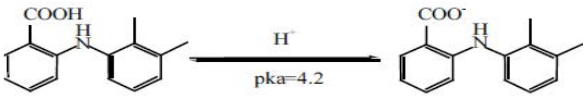


(6)

In an alkaline environment, Cu-doped $TiO_2$ gains a negative charge in that way electro attracting forces can exist between the $TiO_2$ surface and the MFA cations in the solution increasing the adsorption of these cations onto the solar irradiated surface of Cu-doped $TiO_2$ and hence boosting the MFA degradation. On another hand, the inverse trend was seen in acidic media. This may be due to the repelling electrostatic forces between $TiO_2$ nanoparticles and MFA ions in the suspension retarding the adsorption onto the Cu-doped $TiO_2$. Poulios and Tsachpinis [26] presented Eqs. (7) and (8) describing the variation of the characteristics of $TiO_2$ surface with changing pH of the wastewater in the neighbor of its $pH_{pzc}$.

$$TiOH + H^+ \rightleftarrows TiOH_2^+ \qquad pH < pH_{pzc} \quad (7)$$

$$TiOH + OH^- \rightleftarrows TiO^- + H_2O \qquad pH < pH_{pzc} \quad (8)$$

One may conclude that pH variations affect the adsorption of MFA cations over the $TiO_2$ surface, a paramount move for the photooxidation to occur. For our Cu-doped $TiO_2$ photocatalyst, $pH_{pzc}$ is between 5.9 and 6.2. So, when solution pH is more than 6.2 the adsorbed cations of MFA onto the $TiO_2$ start to increase due to the increase of $TiO^-$ groups on the $TiO_2$ surface. In the present work, %$R$ attained maxima at pH = 10. Due to this, the photolysis of MFA achieves higher values in alkaline environments as pH being varied from 7 to 10 [26,27].

### 3.5.2. Effect of $H_2O_2$ loading

Fig. 10 illustrates the influence of various $H_2O_2$ additions (300–800 mg $L^{-1}$ on %$R$ of MFA under incident irradiation of solar energy, when other operating variables kept constant, at reactor effluent after 90 min. As can be seen in Fig. 10, as $H_2O_2$ loading varied from 300, 400, 500, and 800 mg $L^{-1}$ the percentage degradation become 91%, 97.5%, 82%, and 68%, respectively, at 90 min of treatment. As can be shown in Fig. 8, that as the $H_2O_2$ loading was increased,

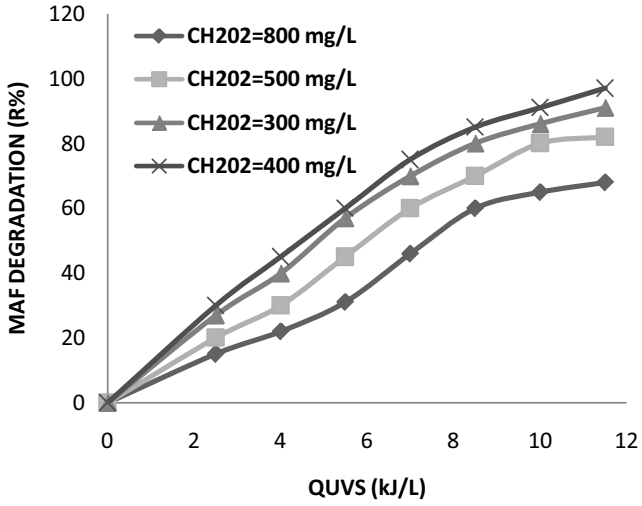


Fig. 10. Variation of %*R* against $Q_{UVS}$ at different $H_2O_2$ loading at reactor effluent after 90 min.

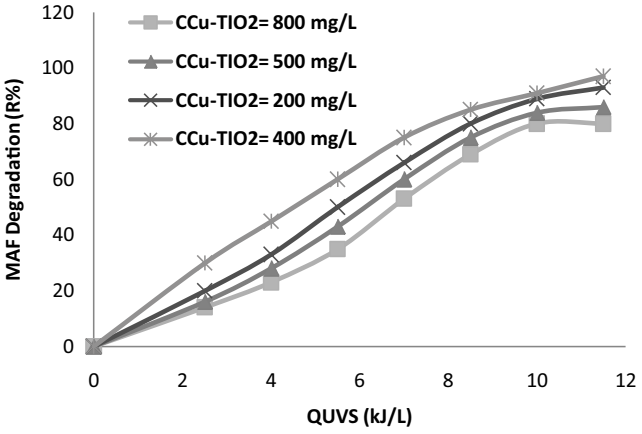


Fig. 11. Variation of %*R* against $Q_{UVS}$ for different photocatalyst loadings at reactor effluent after 90 min.

%*R* for MFA followed the same trend approaching the highest value at $H_2O_2$ loading of 400 mg $L^{-1}$ and beyond this %*R* began to decline with more loading of $H_2O_2$. This may be concluded that the better $H_2O_2$ loading for %*R* is 400 mg $L^{-1}$ which was applied for all setup runs. The above behavior may be attributed to that at a small loading of $H_2O_2$ an insufficient amount of •OH radicals which is responsible for MFA degradation, was forming. In addition, $H_2O_2$ has an importance in the suppression of the recombination of $e^-$–$h^+$ pairs onto the $TiO_2$ surface, enhancing the forming of •OH over the catalyst [28]. On another hand, as the $H_2O_2$ loading boosted beyond 400 mg $L^{-1}$, the rising in %*R* becomes less. This is owing to the fact that if a larger amount of $H_2O_2$ was loaded a higher amount of •OH radicals are being generated. The excess in •OH radicals over that required for the photooxidation reaction prefers to interact with the surplus of $H_2O_2$ instead of interacts with the MFA [7]. It appears that $H_2O_2$ has two functions in photooxidation reaction, firstly it performs as an electron gainer and it may also be dis-bonded to generate •OH [29].

### *3.5.3. Effect of degree of suspension*

Alteration of %*R* vs. incident solar energy for different $TiO_2$ loading (300–800 mg $L^{-1}$) keeping other operating variables constant is shown in Fig. 11. It is observed in Fig. 11 that, each certain amount of suspended $TiO_2$ in wastewater the percentage of degraded MFA increased steeply with the accumulated incident solar energy until it attained a specific value after then the rate of increasing becoming slower. This behavior may be attributed to the positive relationship of the photooxidation reaction with MFA loading that is the photooxidation reaction rate is being slower when the consumed amount of MFA becomes larger. Fig. 11 illustrates also a progressive increasing effect of $TiO_2$ concentration on %*R;* this tendency may be due to the augmentation of the active site of $TiO_2$ with more MFA cations being surface-adsorbed. Our outcomes have been close to the results of published data [30,31]. With a view to shunning the utilization of surplus $TiO_2$, it is needful to predict the most favorable loading for the effective degradation of MFA. It is seen in Fig. 11 that as $TiO_2$ loading raised from 300 to 400 mg $L^{-1}$ %*R* is being boosted, accordingly. This may be due to the increase in $TiO_2$ active sites which enhanced the photooxidation reaction. On another hand, %*R* is being declined as $TiO_2$ loading raised from 400 to 800 mg $L^{-1}$. This behavior may be due to the limitation of solar light penetration into wastewater due to higher suspension density leading to a lightproof environment [7,30].

### *3.5.4. Effect of wastewater flow rate ($Q_{stw}$)*

Influence of wastewater flow on the %*R* was investigated by variation of wastewater during the laminar flow mode from 0.3 to 1.5 L $min^{-1}$ with other operating variables kept constant at $C_{MFA}$ = 10 mg $L^{-1}$, $C_{Cu-TiO_2}$ = 400 mg $L^{-1}$, $C_{H_2O_2}$ = 400 mg $L^{-1}$, and pH = 10. Fig. 12 depicts the %*R* vs. incident solar energy. As can be shown from Fig. 12, %*R* is affected negatively by the increase in wastewater flow. This may be attributed to the contact time of synthetic wastewater flow with incident solar energy where contact time decreased as the flow rate of suspension increased. It can be deduced from Fig. 12 that at 0.5 L $min^{-1}$ of wastewater, MFA has encountered a percentage degradation of 97.5% at 90 min of solar illumination. When the suspension flow raised to 1.5, 2, 2.5, and 3 L $min^{-1}$, %*R* of the MFA were 80%, 74%, 60%, and 40% respectively. This could be also attributed to the restrictions of the solar light breakthrough as the liquid thickness increased due an increase in suspension flow which results in a reduction of photooxidation performance. MFA percentage degradation vs. Reynolds's number of the suspension flow rate is shown in Fig. 13. The suspension Reynolds number ($N_{Re}$) can be estimated from Eq. (9) [32].

$$N_{Re} = \frac{4Q_{sw}\rho_{sw}}{W\mu_{sw}\cos\beta} \tag{9}$$

where $Q_{sw}$ is the synthetic wastewater flow ($m^3s^{-1}$); $\rho_{sw}$ is the wastewater density ($kgm^{-3}$); *W* is the glass sheet

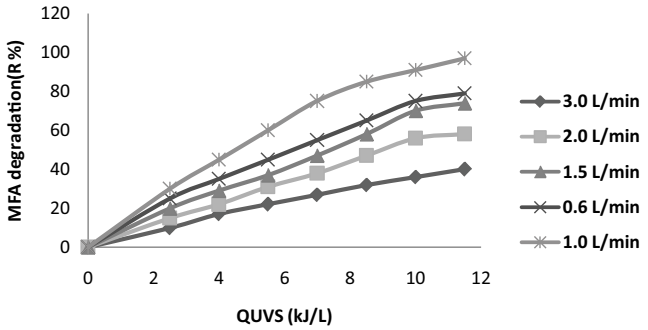


Fig. 12. Variation of the %*R* against $Q_{UVS}$ for different liquid flow rate at reactor effluent after 90 min.

width; $\mu_{sw}$ is the wastewater viscosity (kg $m^{-1}$ $s^{-1}$); and β is the inclined angle. Fig. 13 shows that operating at lower $N_{Re}$ (=138) the wastewater flow was not sufficient to cover all irradiated glass surface and dry batches have been seen during the experimental work, %*R* was low accordingly. As wastewater flow increased covering all irradiated glass surfaces, %*R* attained 97.5% at $N_{Re}$ = 207. However, increasing wastewater flow more gives a reverse response on %*R*. At Reynolds, number 277, 346, and 414 the corresponding %*R* was 82.3%, 61.4%, and 40.32%. This confirmed the influence of liquid flow on contact time between the %*R* and solar illumination.

### *3.5.5. Influence of initial MFA loading*

The influence of initial MFA loading on %*R* has been studied by altering the MFA loading from 10 to 75 mg $L^{-1}$. Fig. 14 illustrates the variation of %*R* vs. MFA loadings with constant operating variables ($C_{H_2O_2}$ = 400 mg $L^{-1}$, $C_{Cu-TiO_2}$ = 400 mg $L^{-1}$, $Q_{sw}$ = 1.0 L $min^{-1}$, and pH = 10) under incident solar energy. As shown in Fig. 14, after 90 min of solar irradiation the percentage degradation was 97.5%, 86.7%, 64.7%, 48.6%, and 35.52% with initial loadings of MFA of 10, 30, 45, 60, and 75 mg $L^{-1}$, respectively. Experiment results depict that as the MFA loading raised, the nondegraded MFA in the suspension increases. This could be attributed to the active site of the photocatalyst which is at certain loading would not be sufficient to degrade the increasing catalyst initial loading. This suggests that as the loading of MFA raised, another operating parameter should be also optimized accordingly to obtain a high %*R* when some other operating variables hold constant. Our outcomes agree well with published data [25].

### *3.5.6. Comparison for catalyst performance between Cu-doped $TiO_2$ and pure $TiO_2$*

A comparison of photocatalyst performance with different Cu-doping (0, 0.5, and 2.5 wt.%) for %*R* vs. $Q_{UVS}$ at optimum operating variables is shown in Fig. 15. As can be seen in Fig. 13, the 2 wt.% Cu doped $TiO_2$ offers a remarkable enhancement on the performance for MFA degradation under incident solar energy. Experimental results revealed that nearly 50.09% of enhancement in MFA degradation was observed for the 2 wt.% Cu-doped $TiO_2$. While $TiO_2$

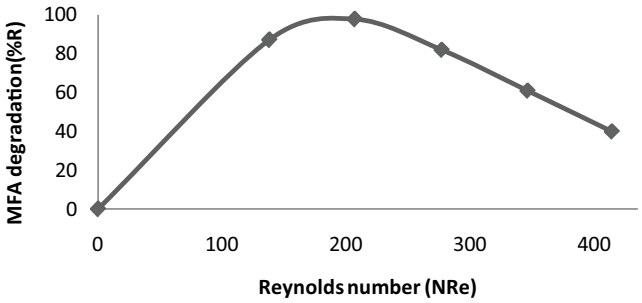


Fig. 13. Variation of %*R* vs. $N_{Re}$.

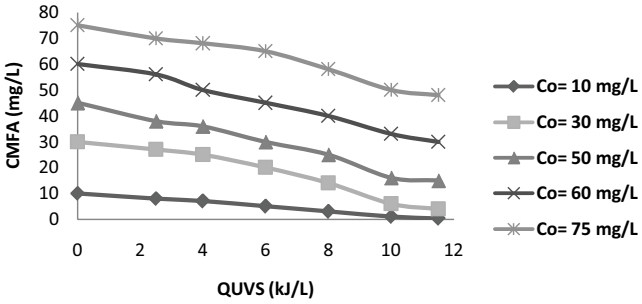


Fig. 14. Variation of initial MFA loading against $Q_{UVS}$ at optimum operating variables.

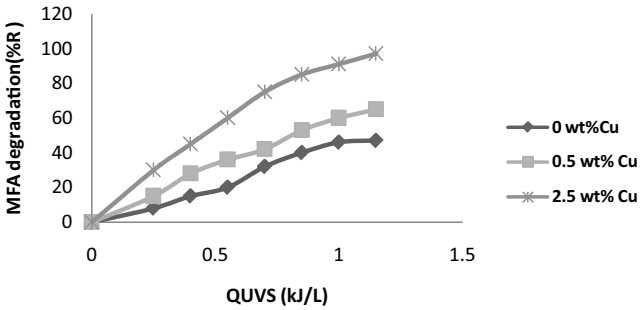


Fig. 15. Comparison of photocatalyst performance with different Cu-doping for %*R* vs. $Q_{UVS}$ at optimum operating variables.

doping with 0.5 wt. Cu offers an average increase in MFA degradation of 32.4% over that of undoped $TiO_2$. This may be attributed to the effect of the Cu powder dispersed onto $TiO_2$ nanoparticles which reduce the bandgap of pure $TiO_2$ (3.2 eV) to 3.04 and 2.2 eV for 0.5 and 2 wt.% of Cu-doped $TiO_2$, respectively. This reduction in the bandgap facilitates the utilizing of the visible light spectrum in addition to the UV spectrum in the photooxidation process [33].

## 4. Conclusion

Experimental results on the removal of MFA in wastewaters under solar irradiation energy revealed that some operating variables such as wastewater acidity, photocatalyst, and hydrogen peroxide loadings, and wastewater flow affects the removal efficacy of MFA in the following descending order, pH > $H_2O_2$ > $TiO_2$ > Flow rate. Adsorption

experiments revealed that the Langmuir isotherm model well described the experimental data.

It was shown that an alkaline environment enhanced the MFA using a falling-film type system under solar illumination. Doping of $TiO_2$ with Cu has a great influence on the enhancement of MFA removal. Using of Cu with 2 wt.% has boosted the removal of MFA by 50.09% because the band-gap of pure $TiO_2$ was reduced from 3.2 to 2.2 by the doping process. All operating variables should be optimized to give better removal efficacy. Increasing $H_2O_2$ loading beyond the optimum value has a disproportionately effect on the removal. While increasing the photocatalyst more than the optima reduced the penetration of solar light through the liquid film.

## References


[1] K. Moribe, R. Kinoshita, K. Higashi, Y. Tozuka, K. Yamamoto, Coloration phenomenon of mefenamic acid in mesoporous silica FSM-16, Chem. Pharm. Bull., 58 (2010) 214–218.

[2] O.S. Al-Khazrajy, A.B.A. Boxall, Risk-based prioritization of pharmaceuticals in the natural environment in Iraq, Environ. Sci. Pollut. Res., 23 (2016) 15712–15726.

[3] S. Daouk, N. Chèvre, C. Vernaz, C. Widmer, Y. Daali, S. Fleury-Souverain, Dynamics of active pharmaceutical ingredients loads in a Swiss university hospital wastewaters and prediction of the related environmental risk for the aquatic ecosystems, Sci. Total Environ., 547 (2016) 244–253.

[4] M. Nassef, S. Matsumoto, M. Seki, F. Khalil, I.J. Kang, Y. Shimasaki, Y. Oshima, T. Honjo, Acute effects of triclosan, diclofenac and carbamazepine on feeding performance of Japanese medaka fish (*Oryzias latipes*), Chemosphere, 80 (2020) 1095–1100.

[5] P. Chen, W. Lv, Z. Chen, J. Ma, R. Li, K. Yao, G. Liu, F. Li, Phototransformation of mefenamic acid induced by nitrite ions in water: mechanism, toxicity, and degradation pathways, Environ. Sci. Pollut. Res., 22 (2015) 12585–12596.

[6] A. Fujishima, X. Zhang, Titanium dioxide photocatalysis: present situation and future approaches, C.R. Chim., 9 (2006) 750–760.

[7] A. Dixit, A.K. Mungray, M. Chakraborty, photochemical oxidation of phenol and chlorophenol by UV/$H_2O_2$/$TiO_2$ process: a kinetic study, Int. J. Chem. Eng. Appl., 1 (2010) 247–250.

[8] Z. Bielan, A. Sulowska, S. Dudziak, K. Siuzdak, J. Ryl, A. Zieli´nska-Jurek, Defective $TiO_2$ core-shell magnetic photocatalyst modified with plasmonic nanoparticles for visible light-induced photocatalytic activity, Catalysts, 10 (2020) 672–692.

[9] L.S. Yoong, F.K. Chong, B.K. Dutta, Development of copper-doped $TiO_2$ photocatalyst for hydrogen production under visible light, Energy, 34 (2009) 1652–1661.

[10] M. Sahu, P. Biswas, Single-step processing of copper-doped titania nanomaterials in a flame aerosol reactor, Nanoscale Res. Lett., 6 (2011) 1–14.

[11] M.F. Abid, I. Mohammed, N. Orroba, H. Luma, M. Neran Maneual, S. Abeer, Designing and operating a pilot plant for purification of industrial wastewater from toxic organic compounds by utilizing solar energy, Korean J. Chem. Eng., 31 (2014) 1194–1203.

[12] M.F. Abid, Desulfurization of gas oil using a solar photocatalytic microreactor, Energy Procedia, 74 (2015) 663–678.

[13] H.P. Shivaraju, N. Muzakkira, B. Shahmoradi, Photocatalytic treatment of oil and grease spills in wastewater using coated N-doped $TiO_2$ polyscales under sunlight as an alternative driving energy, Int. J. Environ. Sci. Technol., 13 (2016) 2293–2302.

[14] R. Shi, Z. Li, H. Yu, Effect of nitrogen doping level on the performance of N-doped carbon quantum dot/$TiO_2$ composites for photocatalytic hydrogen evolution, ChemSusChem, 10 (2017) 4650–4656.

[15] M.F. Abid, S.T. Hamiedi, S.I. Ibrahim, S.K. Al-Nasri, Removal of toxic organic compounds from synthetic wastewater by a solar photocatalysis system, Desal. Water Treat., 105 (2018) 119–125.

[16] O. Gimeno, J. Rivas, A. Encinas, F. Beltran, Application of advanced oxidation processes to mefenamic acid elimination, Int. J. Nucl. Quantum Eng., 4 (2010) 399–401.

[17] K. Sankoda, Y. Sugawara, T. Aida, C. Yamamoto, J. Kobayashi, K. Sekiguchi, Q. Wang, Aqueous photochemical degradation of mefenamic acid and triclosan: role of wastewater effluent matrices, Water Sci. Technol., 79 (2019) 1853–1859.

[18] M. Dolatabadi, S. Ahmadzadeh, M.T. Ghaneian, Mineralization of mefenamic acid from hospital wastewater using electro-Fenton degradation: optimization and identification of removal mechanism issues, Environ. Prog. Sustainable Energy, 38 (2019) 1–10.

[19] K. Krishnaiah, P. Shahabudeen, Applied Design of Experiments and Taguuchi Methods, PHI Learning Private Limited, New Delhi, 2012.

[20] L.X. Ademir, C. Sergio, Black body radiation as a function of frequency and wavelength: an experimentally oriented approach, Rev. Bras. Ensino Física, 34 (2012) 2304–2307.

[21] E.N. Bakatula, D. Richard, C.M. Neculita, G.J. Zagury, Determination of point of zero charge of natural organic materials, Environ. Sci. Pollut. Res. Int., 25 (2018) 7823–7833.

[22] P. Tajana, K. Nikola, Point of zero charge and surface charge density of $TiO_2$ in aqueous electrolyte solution as obtained by potentiometric mass titration, Croat. Chem. Acta, 79 (2006) 95–106.

[23] Y. Geng, J. Zhang, J. Zhou, J. Lei, Study on adsorption of methylene blue by a novel composite material of $TiO_2$ and alum sludge, RSC Adv., 8 (2018) 32799–32807.

[24] A.M. Abodif, L. Meng, S. Ma, A.S.A. Ahmed, N. Belvett, Mechanisms and models of adsorption: $TiO_2$-supported biochar for removal of 3,4-dimethylaniline, ACS Omega, 5 (2020) 13630–13640.

[25] Z. Qianxin, W. Fengliang, Photocatalytic degradation mechanism of mefenamic acid by N-doped carbon quantum dots loaded on $TiO_2$, China Environ. Sci., 37 (2017) 2930–2940.

[26] I. Poulios, I. Tsachpinis, Photodegradation of the textile dye Reactive Black 5 in the presence of semiconducting oxides, J. Chem. Technol. Biotechnol., 74 (1999) 349–357.

[27] C.-Y. Wu, K.-J. Tu, J.-P. Deng, Y.-S. Lo, C.-H. Wu, Markedly enhanced surface hydroxyl groups of $TiO_2$ nanoparticles with superior water-dispersibility for photocatalysis, Materials, 10 (2017) 566–581.

[28] C. Singh, R. Chaudhary, K. Gandhi, Preliminary study on optimization of pH, oxidant and catalyst dose for high COD content: solar parabolic trough collector, Iran. J. Environ. Health Sci. Eng., 10 (2013) 13–23.

[29] N. Guettaï, H.A. Amar, Photocatalytic oxidation of methyl orange in presence of titanium dioxide in aqueous suspension. Part I: parametric study, Desalination, 185 (2005) 427–437.

[30] T. Kojima, T.A. Gad-Allah, S. Kato, S. Satokawa, Photocatalytic activity of magnetically separable $TiO_2$/$SiO_2$/$Fe_3O_4$ composite for dye degradation, J. Chem. Eng. Jpn., 44 (2011) 662–667.

[31] R.B. Bird, W.E. Stewart, E.N. Lightfoot, Transport Phenomena, 2nd ed., John Wiley & Sons, Inc., Singapore, 2002.

[32] I.K. Konstantinou, T.A. Albanis, $TiO_2$-assisted photocatalytic degradation of azo dyes in aqueous solution: kinetic and mechanistic investigations: a review, Appl. Catal., B, 49 (2004) 1–14.

[33] L. Chen, T.B. Nguyen, L. Yi-Li, W. Chung-Hsin, C. Jih-Hsing, C. Chiu-Wen, D. Cheng-Di, Enhanced heterogeneous photodegradation of organic pollutants by a visible light harvesting CoO@meso–CN@$MoS_2$ nanocomposites, Catalysts, 10 (2020) 722–736.